

Another Non-segregated Blue Straggler Population in a Globular Cluster: the Case of NGC 2419⁵

E. Dalessandro^{1,2}, B. Lanzoni¹, F.R. Ferraro¹, F. Vespè², M. Bellazzini³, R.T. Rood⁴

ABSTRACT

We have used a combination of *ACS-HST* high-resolution and wide-field *SUB-ARU* data in order to study the Blue Straggler Star (BSS) population over the entire extension of the remote Galactic globular cluster NGC 2419. The BSS population presented here is among the largest ever observed in any stellar system, with more than 230 BSS in the brightest portion of the sequence. The radial distribution of the selected BSS is essentially the same as that of the other cluster stars. In this sense the BSS radial distribution is similar to that of ω Centauri and unlike that of all Galactic globular clusters studied to date, which have highly centrally segregated distributions and, in most cases, a pronounced upturn in the external regions. As in the case of ω Centauri, this evidence indicates that NGC 2419 is not yet relaxed even in the central regions. This observational fact is in agreement with estimated half-mass relaxation time, which is of the order of the cluster age.

Subject headings: Globular clusters: individual (NGC 2419); stars: evolution – Horizontal Branch - binaries: general - blue stragglers

1. INTRODUCTION

This paper is part of a series aimed at studying the complex interplay between dynamics and stellar evolution in a sample of globular clusters (GCs) with different structural properties. To this purpose we are using the so-called Blue Stragglers Star (BSS) population as

¹Dipartimento di Astronomia, Università degli Studi di Bologna, via Ranzani 1, I-40127 Bologna, Italy

²ASI, Centro di Geodesia Spaziale, contrada Terlecchia, I-75100, Matera, Italy

³INAF–Osservatorio Astronomico di Bologna, via Ranzani 1, I-40127 Bologna, Italy

⁴Astronomy Department, University of Virginia, P.O. Box 400325, Charlottesville, VA, 22904

⁵Based on observations with the NASA/ESA *HST*, obtained at the Space Telescope Science Institute, which is operated by AURA, Inc., under NASA contract NAS5-26555. Also based on SUBARU observations collected at the Hawaii National Astronomical Observatoty of Japan.

a probe. BSS are the most abundant and common population of stars which significantly deviates from the evolutionary path defined by a simple, old stellar population. In the Color Magnitude Diagram (CMD), BSS define a sparsely populated sequence more luminous and bluer than the Turn-Off point (TO) of a normal hydrogen-burning main-sequence (MS). Hence they appear as stars more massive (see also Shara et al. 1997) and younger than the bulk of the cluster population. They are thought to form from the evolution of binary systems, either via mass-transfer/coalescence phenomena in primordial binaries (PB-BSS; McCrea 1964; Zinn & Searle 1976), or by stellar mergers induced by collisions (COL-BSS; Hills & Day 1976). Since collisional stellar systems like GCs dynamically evolve over a time-scale significantly shorter than their age, BSS are expected to have sunk into the cluster core, as have the majority of the most massive objects (like binaries and other binary by-products) harbored in the system.

In many GCs the projected radial distribution of BSSs has been found to be bimodal: highly peaked in the center, with a clear-cut dip at intermediate radii, and with an upturn in the external regions. Such a behavior has been confirmed in at least 7 GCs: M3, 47 Tuc, NGC 6752, M5, and M55, NGC 6388 (all references in Dalessandro et al. 2007) and M53 (Beccari et al. 2008). Dynamical simulations (Mapelli et al. 2006; Lanzoni et al. 2007a,c) suggest that the observed central peak is mainly due to COL-BSS formed in the core and/or PB-BSS sunk into the center because of dynamical friction, while the external rising branch is made of PB-BSS evolving in isolation in the cluster outskirts. Even in those GCs that do not show any bimodality the BSS always appear to be significantly more segregated in the central regions than the reference cluster stars. The only exception to these general observational features is ω Centauri (hereafter ω Cen): the large population of BSS discovered by Ferraro et al. (2006, hereafter F06) in this giant stellar system has the same radial distribution of the normal cluster stars. This is a clear evidence that ω Cen is not fully relaxed, even in the central regions, and therefore, the dynamical evolution of the cluster has not significantly altered the radial distribution of these stars. It is likely that the vast majority of BSS observed in this cluster are the progeny of primordial binaries evolved in isolation (see also Mapelli et al. 2006).

Here we direct our attention to another massive cluster (NGC2419) which shares a number of properties with ω Cen. This remote object ($d \sim 81$ kpc; Harris et al. 1997) is one of the most luminous clusters in the Galaxy ($M_V = -9.4$; see Bellazzini 2007, hereafter B07), similar to ω Cen and M54 (NGC 6715). It has been suggested that both of the latter clusters are the remnants of stripped cores of dwarf spheroidals (see, e.g., Layden & Sarajedini 2000; Bekki & Freeman 2003). With its high luminosity and half-light radius ($r_h \simeq 25$ pc; B07), NGC 2419 lies (together with ω Cen and M54) in the (r_h, M_V) plane well above the locus defined by all the other Galactic GCs. Indeed, it is the most significant outlier, thus

suggesting that it also might be the stripped core of a former dwarf galaxy (van den Bergh & Mackey 2004; Mackey & van den Bergh 2005). Further, Newberg et al. (2003) suggested that NGC 2419 could be somehow connected with the Sagittarius (Sgr) dwarf spheroidal, since it seems to be located in a region with an overdensity of type-A stars which is in the same plane as the tidal tails of Sgr. However, the high-quality CMDs of NGC 2419 recently published by Ripepi et al. (2007, hereafter R07; see also B07) do not show any evidence of multiple stellar populations, in contrast to ω Cen (Lee et al. 1999; Pancino et al. 2000; Bedin et al. 2004; Rey et al. 2004; Sollima et al. 2005) and possibly M54 (Layden & Sarajedini 2000; see also Monaco et al. 2005). It is however possible that for such a metal-poor cluster ($[Fe/H] = -1.97$; Ferraro et al. 1999b), the range in metallicities for the sub-population components is so small that different sequences cannot be seen in the CMD (Mackey & van den Bergh 2005; Federici et al. 2007).

In order to further investigate the dynamical status and the stellar populations of this remote cluster, here we present a multi-wavelength study of BSS in NGC 2419. By combining HST high-resolution data, with wide-field SUBARU images, we sampled the total radial extension of the cluster. This allowed us to study and compare the projected radial distributions of BSS and other cluster stars in different evolutionary stages. The data and photometric reductions are described in § 2. A general overview of the CMD is discussed in § 3. The BSS population is described in § 4, and the Discussion is presented in § 5.

2. OBSERVATIONS AND DATA ANALYSIS

2.1. The data sets

To study the crowded cores of high-density systems and simultaneously cover the total cluster extensions, a combination of high resolution observations of the central regions and complementary wide-field images is needed.

1. High resolution set – This is composed of a series of public images obtained with the Wide Field Channel of the Advanced Camera for Surveys (ACS) on board the Hubble Space Telescope (HST): two F435W ($\sim B$ filter) images with $t_{\text{exp}} = 800$ sec each, two F555W ($\sim V$ filter) images with $t_{\text{exp}} = 720$ sec, and two F814W ($\sim I$ filter) images with $t_{\text{exp}} = 676$ sec (Prop GO9666, P.I. Gilliland). These are the highest resolution ($\sim 0.05'' \text{ pixel}^{-1}$) observations available to date for NGC 2419. Unfortunately the ACS images are off-centered (see Figure 1), and they do not completely sample the most central region of the cluster. As in previous works (see, e.g., Dalessandro et al. 2007), average ACS images were obtained in each filter, and they were corrected for geometric distortion and effective flux (Sirianni et al.

2005). The data reduction has been performed using the ROMAFOT package (Buonanno et al. 1983), specifically developed to perform accurate photometry in crowded regions (Buonanno & Iannicola 1989).

2. *Wide field set* – We have used a set of public V and I images obtained with the SUBARU Prime Focus Camera (Suprime-Cam) of the 8.2m SUBARU telescope at the Hawaii National Astronomical Observatoty of Japan. The Suprime-Cam is a mosaic of ten 2048×4096 CCDs, which covers a $34' \times 27'$ field of view (FoV) with a pixel scale of $0.2''$. A combination of long-exposures ($t_{\text{exp}} = 180$ sec) and median exposure ($t_{\text{exp}} = 30$ sec) images has been retrieved from the Subaru Archive Web site (SMOKA). As shown in Figure 2, the cluster is centered in the chip #2 and it is totally included in the five adjacent chips; therefore only these six chips have been considered in the present study. We have applied standard pre-reduction procedures (correction for bias, flat-field and overscan) using IRAF¹ tools. The reduction was performed independently for each image using the PSF fitting software DoPhot (Schechter et al. 1993).

2.2. Astrometry, center of gravity and photometric calibration

The ACS and SUBARU data have been placed on the absolute astrometric system by using the stars in common between each single chip and the SDSS data set used by B07, that, in turn, was astrometrized on the GSC-II astrometric reference star catalog. Hundreds of stars have been matched in each chip, thus allowing a very precise determination of the stellar absolute positions. The resulting rms residuals (a measure of the internal astrometric accuracy) were of the order of $\sim 0''.3$ both in Right Ascension (α) and Declination (δ).

The photometric calibration of the ACS catalog has been performed in the VEGAMAG system using the relations and zero-points described in Sirianni et al. (2005). Then, the SUBARU catalog has been homogenized to the ACS one. In order to transform of the instrumental SUBARU magnitudes into the ACS VEGAMAG system, a subsample of a few hundred stars in common between the SUBARU and the ACS FoVs has been selected, and the following relations have been obtained:

$$I_{\text{ACS}} - i_{\text{SUBARU}} = -0.55 \times (V - I)_{\text{ACS}} + 27.41 \quad (1)$$

$$V_{\text{ACS}} - v_{\text{SUBARU}} = -0.20 \times (V - I)_{\text{ACS}} + 27.46 \quad (2)$$

¹IRAF is distributed by the National Optical Astronomy Observatory, which is operated by the Association of Universities for Research in Astronomy, Inc., under cooperative agreement with the national Science Foundation

where i_{SUBARU} and v_{SUBARU} are the instrumental I and V magnitudes in the SUBARU sample referred to 1 second exposure. In this way a final list of absolute positions and homogeneous (VEGAMAG) magnitudes for all the stars in the two catalogs was obtained.

In order to determine the Center of Gravity (C_{grav}) of the cluster, we have computed the barycenter of all the stars found in the ACS catalog at a distance $r < 10''$ from the center quoted by Harris (1996). A circular region of $10''$ radius is the maximum available area completely covered by the ACS observations (see Fig.1). The absolute positions (α , δ) of the stars have been averaged using an iterative technique described in previous works (e.g., Montegriffo et al. 1995; Ferraro et al. 2003). We have excluded stars brighter than $V = 19.5$ since they are saturated in the ACS images. The same procedure has been repeated for three different magnitude cuts ($V < 24$, $V < 23.5$, and $V < 23$) in order to check for any possible statistical or spurious fluctuations. The three measures agree within $\sim 1''$ and their mean value has been adopted as best estimate of C_{grav} : $\alpha = 7^{\text{h}} 38^{\text{m}} 8^{\text{s}}.47^{\text{s}}$ and $\delta = 38^{\circ} 52' 55''.0$, with an uncertainty of $0''.5$ in both α and δ . This new determination is in agreement with that listed by Harris (1996).

Given the coordinates of C_{grav} , we have divided the dataset in two main samples: the *HST sample*, which includes all the stars found in the ACS catalog, and the *SUBARU sample*, that consists of stars not included in the ACS FoV and lying at $r > 60''$ from the cluster center. The latter choice implies that a small region (a segment of a circle located $\sim 20''$ North from the cluster center) is covered neither by the HST nor by the SUBARU sample (see Fig.2). This conservative choice is made to avoid incompleteness effects of the ground based observations in the most crowded central regions of the cluster.²

3. CMD overall characteristics and the HB morphology

The CMD of stars in the HST sample is shown in Figure 3. This is the deepest CMD ever published for NGC 2419, reaching down to $B \sim 27$. All the main cluster evolutionary sequences are clearly defined and well populated. The stars in the brightest ($B < 19.5$) portion of the red giant branch (RGB) are not shown in the figure, because they are heavily saturated in these exposures. The MS-TO of the cluster is located at $B_{\text{TO}} = 24.5 \pm 0.1$. Particularly notable is the horizontal branch (HB) morphology, which looks quite complex, with a long HB blue tail (BT) extending well below the cluster MS-TO. The peak of the HB population is located at $B \sim 20.7$ and $(B - I) \sim 0.2$. The HB population significantly

²However, note that the annular region between $20''$ and $60''$ from the cluster center is well sampled (at $\sim 70\%$) by the ACS sample.

decreases with decreasing luminosity along the BT. A poorly populated region (a gap?) is visible at $B \sim 23.4$, separating the extreme extension of the BT and a clump of stars extending down to $B \sim 25$. Following the nomenclature adopted in Dalessandro et al. (2007), these are extreme HB (EHB) stars with the faintest ones being Blue Hook (BHk) stars. Definitive assignment to these groups will require UV photometry.

In Figure 4 we show a direct comparison between the HB of NGC 2419, and that of ω Cen (from Ferraro et al. 2004), suitably shifted (by ~ 5.6 magnitudes) in order to match the HB level of NGC 2419. The two HBs show very similar extension and morphology. The only significant difference is that EHB/BHk stars in NGC 2419 are much more spread-out in color $\delta(B - I) \sim 1$ than the same population in ω Cen. The rms scatter between the magnitude measurements in the two single images, is $\sigma_B \sim 0.1$ and $\sigma_I \sim 0.24$ mag in the B and I bands, respectively. Thus the photometric error in $(B - I)$ is $\sigma_{B-I} \sim 0.26$ mag at the level of BHk stars. The observed color spread is about 4σ and may thus be real. To demonstrate more clearly the striking similarity of these HBs, in Figure 5 we show the normalized B magnitude distribution of HB stars. The percentage of stars in three portions of the branch is also designated in the figure. Beyond general appearance, the HBs are quantitatively similar: (i) both the HBs extend for almost 4.5 mag; (ii) both the distributions show a well defined peak, an extended tail and a EHB/BHk clump; (iii) the bulk of the HB population ($\sim 58\%$) is localized in the brightest 1 magnitude portion of the branch; (iv) the BT is 10–12% of the population; (v) both the EHB/BHk clumps extend for roughly 1.5 magnitudes and they comprise $\sim 30\%$ of the total HB population.

As discussed in Dalessandro et al. (2007), the nature of BHk stars is still unclear: they may be related to the so-called late hot flashers (Moehler et al. 2004, Catelan 2007), or due to high helium abundances (as suggested by Busso et al. 2007, in the case of NGC 6388; see also Caloi & D’Antona 2007; D’Antona et al. 2005), or related to the evolution of binary systems (Heber et al. 2002). However, the detection of a population of BHk stars in a low-metallicity cluster as NGC 2419 clearly demonstrates that the process producing these extremely hot HB stars can efficiently work in any metallicity environment: NGC 6388 ($[Fe/H] \sim -0.4$), NGC 2808 ($[Fe/H] \sim -1.1$), ω Cen ($[Fe/H] \sim -1.6$), M54 ($[Fe/H] \sim -1.8$) and NGC 2419 ($[Fe/H] \sim -2$). It is interesting to note that NGC 2419 is very massive as are the other BHk clusters. We have also checked the EHB/BHk radial distributions with respect to the brightest portion of the HB and the RGB. The significance of the difference has been quantified with a Kolmogorov-Smirnov (KS) test: the radial distribution of the BHk population is consistent with that of normal cluster stars, in agreement with similar findings in NGC 6388 (Rich et al. 1997, Dalessandro et al. 2007) and ω Cen (Ferraro et al. 2004). However, the evidence presented in Sect. 4.2 demonstrate that NGC 2419 is not relaxed even in the central regions, hence no segregation is expected for these stars even

in the case they were binaries. Moreover, as discussed in Dalessandro et al. (2007), it is important to remember that the lack of segregation of the EHB/BHk population is not a firm proof of the non-binarity of EHB/BHk stars, since they could be low-mass binaries, with a total mass similar (or even lower) than “normal” cluster stars (for example, a $0.5 M_{\odot}$ He-burning star with a $0.2 M_{\odot}$ He white dwarf companion).

3.1. Density profile and distance modulus estimate

The $(V, V - I)$ CMDs of the HST and SUBARU samples defined in Section 2.2 are shown in Figure 6. Thanks to the high-resolution ACS images of the cluster core and the wide FoV of the SUBARU observations, we have properly sampled the stellar population over the entire cluster extension. We have then used this data-set to determine the projected density profile of NGC 2419 using direct star counts, from C_{grav} out to about $1000''$.

Stars with $V < 19.5$ are saturated in the ACS sample and therefore have been excluded from the analysis; however, since they are small in number, this produces a negligible effect on the global result. In order to avoid incompleteness biases we have also excluded stars fainter than $V = 23.5$. Using the same procedure described in Ferraro et al. (1999a) the whole sample has been divided in 24 concentric annuli, each centered on C_{grav} and suitably split in a number of subsectors. The number counts have been calculated in each subsector and the corresponding densities were obtained dividing them by the sampled area (taking into account the incomplete spatial coverage of the region between $20''$ and $60''$). The stellar density of each annulus has then be defined as the average of the subsector densities and its standard deviation is computed from the variance among the subsectors. The resulting projected surface density profile is plotted in Figure 7. As apparent, the outermost two points show a flattening of the stellar number density, and their average (corresponding to $\sim 4 \text{ stars/arcmin}^2$) has therefore been used as an estimate of the background contribution. The derived radial density profile is well fit by an isotropic single-mass King model (solid line in Fig. 7), with concentration $c = 1.36$ and core radius $r_c = 20''$, yielding a “formal” value of the cluster tidal radius of $r_t \sim 460''$ and a half-mass radius of $r_h \sim 58''$. These parameters are essentially equal to those obtained by B07 and in good agreement with other previous determinations (see, e.g., Table 2 in B07).

We have used the available high-quality data set also for deriving an independent estimate of the distance to NGC 2419. To do this, we compared the CMD shown in Fig. 3, to that of M92 (NGC 6341), one of the “prototype” Galactic GCs, with similar metallicity ($[\text{Fe}/\text{H}] \sim -2$, Ferraro et al. 1999b). We have used a combination of WFPC2 and ACS data of M92 (F.R. Ferraro et al. 2008, in preparation), obtained through filters F555W ($\sim V$) and

F814W ($\sim I$). We have shifted the CMD of M92 onto that of NGC 2419 until a good match between the main evolutionary sequences (RGB, HB, sub-giant branch and TO region) of the two clusters was reached (see Figure 8). This has required a color shift $\delta(V - I) = 0.14$ and $\delta V = 5.25$, similar to that obtained by Harris et al. (1997) from an analogous comparison based on independent data sets. Figure 8 shows that a really nice matching of all the evolutionary sequences of the two clusters can be achieved. This evidence also suggests that the two clusters have a similar age (in agreement with Harris et al. 1997, who estimated an age difference of ~ 1 Gyr for the two objects).

By assuming the distance modulus $(m - M)_0 = 14.78$ and the reddening $E(B - V) = 0.02$ for M92 (Ferraro et al. 1999b), and by using the standard absorption coefficient ($A_V = 3.1$ and $A_I = 1.7$), we have obtained $E(B - V) = 0.12 \pm 0.03$ and $(m - M)_V = 20.09$, corresponding to a true distance modulus $(m - M)_0 = 19.72$, for NGC 2419. The reddening obtained from this procedure is in good agreement with the value derived by Harris et al. (1997), who quoted $E(B - V) = 0.11$, and it is also in agreement with the value $E(B - V) = 0.08$ adopted by R07 within the errors. Taking a conservative estimate of $\sigma \sim 0.1$ mag, we finally adopt $(m - M)_0 = 19.7 \pm 0.1$. This yields a real distance $d \simeq 87 \pm 4$ kpc. Within the uncertainties, this estimate is in agreement with both that found by Harris et al. (1997; $d = 81 \pm 2$ kpc) and that obtained by R07 using the mean luminosity of the RR Lyrae stars ($d = 83.2 \pm 1.9$ kpc). Assuming this distance, the physical dimension of the core radius and of the half-mass radius of the cluster can be obtained: given $r_c = 20''$ and $r_h = 58''$ (see above), we obtain $r_c = 8.4$ pc and $r_h = 24.5$ pc, respectively. By adopting the total integrated magnitude $V_t = 10.47$ quoted by B07, the absolute cluster magnitude is $M_V = -9.6$. This value, combined with the size of the half-mass radius, confirms the anomalous position of NGC 2419 in the r_h versus M_V plane (van den Bergh & Mackey 2004).

4. THE POPULATION OF BSS

4.1. Population selection

To select the BSS population we have chosen to use the $(B, B - I)$ CMD, in which the BSS sequence is better defined. To avoid spurious effects due to sub-giant branch star blends and Galaxy field star contamination, only stars brighter than $B \simeq 23.6$ (corresponding to ~ 1 mag above the TO) and with $B - I < 0.75$ have been selected (see Figure 9). The resulting number of candidate BSS in the *HST sample* is 183. The position of the bulk of these stars in the ACS $(V, V - I)$ CMD has then been used to define the BSS selection box for the *SUBARU sample*. This is shown in Figure 10, with the faint and red edges corresponding to $V \simeq 23.3$ and $V - I < 0.48$, respectively. The resulting number of candidate BSS found

in the entire SUBARU sample is 67, out of which 49 are found within the “safe” distance of $\sim 500''$ from the cluster center. This distance is slightly larger than the “formal” tidal radius obtained in Sect. 3.1 and takes into account possible uncertainties in the determination of the latter. The positions and magnitudes of the all the 232 candidate BSS thus selected are listed in Table 1, which is available in full size in electronic form.³

Reference populations representative of the “normal” cluster stars are needed to properly study the BSS radial distribution. We considered both the HB and the RGB. Since the HST and the SUBARU samples have the V and I filters in common, we performed a homogeneous selection of these populations in the $(V, V - I)$ plane. The HB selection box (see Fig. 10) has been drawn to limit the contribution of field contamination in the bright-red portion of the sequence (i.e., we have required that $V - I < 0.65$ at $V \sim 20$) and in order to exclude the EHB/BHk clump ($V \gtrsim 23.6$). The EHB/BHk stars populate a region located ~ 1 magnitude below the MS-TO (see Fig. 8), which is very close to the detection limit of the V and I observations. Thus, they could be severely affected by incompleteness bias, and we have therefore preferred not to include them in the HB reference population. However, since their radial distribution is indistinguishable from that of the other HB stars, this exclusion has negligible effect on the following results. The total number of HB stars thus selected within $500''$ is 765, with 528 found in the HST sample and 237 in the SUBARU one. The RGB population has been selected along the RGB mean ridge line between $V \simeq 19.9$ and $V \simeq 22.5$ (see the selection box in Fig. 10). This choice has been dictated by the fact that the brightest portion of the RGB sequence is saturated in the HST sample, and its faintest portion is contaminated by Galactic field stars, especially in the SUBARU sample. The total number of these stars within $500''$ is 3250, with 2337 found in the HST sample and 913 in the SUBARU one.

4.2. BSS radial distribution

A first qualitative comparison between the cumulative radial distribution of BSS and that of the reference populations (see Figure 11) has been performed using the KS test. This gives 70% and 50% probabilities that the BSS population is extracted from the same population as the HB and RGB stars, respectively. Hence there is preliminary evidence that the radial distribution of BSS is indistinguishable from that of the “normal” cluster population, in contrast to what found in most of the typical GCs (see references in Dalessandro et al.

³Several SX Phoenicis variables have been found by R07. However a direct comparison between these stars and our BSS sample is not possible, since the R07 catalog is not yet published.

2007).

For a more detailed analysis, we have used the same technique described in previous works (see, e.g., F06). The sampled area within $r = 500''$ has been divided in 5 concentric annuli centered on C_{grav} . In each of these we have counted the number of BSS, HB and RGB stars. However, the examination of the external regions ($r > 500''$) of the SUBARU sample CMD suggests that the selected (BSS, HB, and RGB) populations can be affected by contamination from stars in the Galactic field. In order to account for this effect we adopted the statistical correction as used in previous papers (see, e.g., Dalessandro et al. 2007). To do this we selected a rectangular region of $\sim 70 \text{ arcmin}^2$ located at $r > 650''$, i.e. well beyond the formal tidal radius of the cluster. The CMD of this region clearly shows that the Galaxy field population is dominant relative to the cluster one. Then we counted the number of stars in this region lying in the BSS, HB and RGB selection boxes showed in Fig. 6 and derived the following values of the field star densities: $D_{\text{BSS}}^{\text{field}} = 0.03 \text{ stars arcmin}^{-2}$, $D_{\text{HB}}^{\text{field}} = 0.06 \text{ stars arcmin}^{-2}$ and $D_{\text{RGB}}^{\text{field}} = 0.14 \text{ stars arcmin}^{-2}$. These quantities allow us to estimate the impact of the field contamination on the selected samples: 6 BSS ($\sim 2\%$), 12 HB ($\sim 1.5\%$) and 31 RGB ($\sim 1\%$), essentially all in the most external annulus, could be field stars (see Table 2). Though the effect of the field contamination is small, in the following we use the statistically decontaminated samples in order to determine the population ratios and the radial distribution.

By using the King model, the distance modulus and the reddening estimated in Sect. 3.1, the luminosity sampled in each annulus (L^{samp}) has also been estimated. Then for each annulus we have computed the double normalized ratio defined in Ferraro et al. (1993):

$$R_{\text{pop}} = \frac{N_{\text{pop}}/N_{\text{pop}}^{\text{tot}}}{L^{\text{samp}}/L_{\text{tot}}^{\text{samp}}}, \quad (3)$$

with pop= BSS, HB and RGB. We find that R_{HB} and R_{RGB} are essentially constant and close to unity (see R_{HB} in Figure 12). This is what expected for any post-MS population according to the stellar evolution theory (Renzini & Fusi Pecci 1988). Surprisingly we also find that the double normalized ratio of BSS is constant, and it is fully consistent with the reference populations (Fig. 12). Using the number counts listed in Table 2, we have also computed the specific frequencies $N_{\text{BSS}}/N_{\text{HB}}$, $N_{\text{BSS}}/N_{\text{RGB}}$ and $N_{\text{HB}}/N_{\text{RGB}}$. We find that all these ratios are almost constant all over the entire extension of the cluster (see Figure 13), confirming again that no signatures of mass segregation are visible for the BSS population of NGC 2419.⁴

⁴Note that this result is independent of which portion of the RGB is selected. In fact, similar results are obtained also by considering the RGB in the same magnitude range of the BSS.

5. DISCUSSION

In most previously surveyed Galactic GCs (M3; 47 Tuc, NGC 6752, M5, M55, NGC 6388, M53) the BSS radial distribution has been found to be bimodal (highly peaked in the core, decreasing to a minimum at intermediate radii, and rising again in the external regions). The mechanisms leading to bimodal radial distributions have been studied for some clusters using dynamical simulations (see Mapelli et al. 2004, 2006; Lanzoni et al. 2007a,c): the observed central peak is mainly made up of collisionally formed BSS and/or PB-BSS sunk into the core because of dynamical friction; the external rising branch is composed of PB-BSS evolving in isolation in the cluster outskirts. In contrast, the BSS radial distribution of NGC 2419 is essentially the same as that of the other “normal” stars in the cluster. Previously, ω Cen was the only GC known to have a flat BSS radial distribution. F06 (see also Meylan & Heggie 1997) argued that two-body relaxation had not led to the complete relaxation of ω Cen even in the central core. Our result here suggests that the same situation holds for NGC 2419.

We can compare this observational evidence with theoretical time-scales expected on the basis of the cluster structural parameters. Following equation (10) of Djorgovski (1993), we computed the cluster central relaxation time (t_{r_c}) by adopting $m = 0.3 M_\odot$ for the average stellar mass, and $M/L = 3$ for the mass-to-light ratio and $M_{V\odot} = 4.79$ for the V band solar magnitude. The integrated magnitude obtained in Sect. 3.1 then leads to a total cluster mass of $1.7 \times 10^6 M_\odot$, and a total number of stars of 5.7×10^6 . By assuming $\rho_0 \simeq 25 M_\odot \text{pc}^{-3}$ (Pryor & Meylan 1993), and given the value of the core radius ($r_c = 8.4 \text{pc}$) derived in Sect. 3.1, we obtain $t_{r_c} \sim 6 \text{Gyr}$, which is about half the cluster age ($t = 12\text{--}13 \text{Gyr}$; Harris et al. 1997). Thus some evidence of mass segregation should be visible at least in the core, at odds with the observed flat distribution of BSS. We can also compute the characteristic relaxation time-scale for stars as massive as BSS ($M_{\text{BSS}} \sim 1.2 M_\odot$; see F06) at the cluster half-mass radius (r_h) using equation (10) of Davies et al. (2004). Since $r_h \sim 24.5 \text{pc}$ (see Sect. 3.1) we obtain $t_{r_h} \sim 18 \text{Gyr}$, thus suggesting that no significant segregation is expected for stars as massive as the BSS in the outer parts of the clusters, in agreement with our observational results. This result is similar to that found for ω Cen by F06 where the relaxation time in the core was found to be \sim half the cluster age. In the case of ω Cen a number of possible explanations were examined; for instance, the possibility that ω Cen is the relic of a partially disrupted galaxy, which was much more massive in the past. A similar argument can be advocated for NGC 2419, which has also been suspected to be the relic of a small dwarf galaxy interacting with the Milky Way (van den Bergh & Mackey 2004; Federici et al. 2007 and references therein). However, it should be noted that the above estimates of the relaxation times are rough, and since the predicted value of t_{r_c} is only a factor of 2 smaller than the cluster age, more detailed computations are needed before further interpret these results.

From the observational side, the BSS radial distribution shown in Figs. 12 and 13 suggests that in NGC 2419 (as in ω Cen) stellar collisions have played a minor (if any) role in modifying the radial distribution of massive objects and probably also in generating exotic binary systems. If dynamical evolution plays a central role in NGC 2419, the observed flat BSS distribution can be explained only by invoking an *ad hoc* formation/destruction rate balancing the BSS population in the core and in the outer region of the cluster. It is more likely that this flat distribution arises because the BSS we are observing result from the evolution of primordial binaries whose radial distribution has not been altered by the dynamical evolution of the cluster. Thus, as in the case of ω Cen, the BSS population observed in NGC 2419 could be a pure population of PB-BSS, and it can be used to evaluate the incidence of such a population in stellar systems.

As in previous papers (see e.g. Ferraro et al. 1995, F06) here we compute the PB-BSS frequency as the number of BSS normalized to the sampled luminosity in units of $10^4 L_{\odot}$: $S4_{\text{PB-BSS}} = N_{\text{BSS}}/L_4$ (see the bottom panel of Fig. 13). This quantity is useful for estimating the expected number of BSS generated by PBs for each fraction of the sampled light in any stellar system, resolved or not⁵. For NGC 2419, we find $S4_{\text{PB-BSS}} = 3.1 \pm 0.6$ (see Fig. 13). Before comparing this quantity to that found in ω Cen by F06, we must account for the fact that the adopted BSS selection criteria are different in the two clusters. In NGC 2419 we considered BSS brighter than $B < 23.6$; this threshold corresponds to $B < 18$ at the distance of ω Cen, using the value $\delta B = 5.6$ needed to shift the HB of ω Cen onto that of NGC 2419 (see Fig. 5). By adopting this threshold, 104 BSS are found in the ACS FoV of ω Cen, and by considering the sampled luminosity, we obtain $S4_{\text{PB-BSS}} = 1.6$ for this cluster.⁶ This comparison suggests that the number of BSS per unit sampled light in NGC 2419 is twice as large than that in ω Cen.⁷ Under the hypothesis that the vast majority of these BSS are generated by the evolution of PBs, the different $S4_{\text{PB-BSS}}$ values could result from a different binary frequency in the two clusters, since PB-BSS are expected to strongly depend on the fraction of binaries in the cluster. Indeed the first direct correlation between these two quantities (the binary fraction and the BSS frequency) has been recently detected in a sample of 13 low-density clusters by Sollima et al. (2008). Such a connection strongly

⁵This quantity is also important in evaluating the incidence of creation/destruction rate of BSS in the central region of high-density clusters, where collisions can have played a major role in producing collisional BSS.

⁶Of course, such a value is slightly smaller than that ($S4_{\text{PB-BSS}} = 2$) obtained in F06 by considering the entire sample of BSS with $B < 18.4$

⁷A similar result is obtained if selecting the BSS population of NGC 2419 down to the same threshold used by F06 for the BSS in ω Cen, i.e. $B < 18.4$ (which corresponds to $B = 24$ at the distance of NGC 2419).

supports a scenario in which the evolution of PBs is the main formation channel for BSS in low-density environments.

The case of NGC 2419 further supports the idea that important signatures of the dynamical evolution of the parent cluster are imprinted in the radial distribution of the BSS population: indeed the most recent results collected by our group (see Ferraro et al. 2003, 2006; Lanzoni et al. 2007a,b,c; Dalessandro et al. 2007) are building the ideal data-base from which such signatures can be read and interpreted, and are already confirming this hypothesis.

This research was supported by PRIN-INAF2006, by the Agenzia Spaziale Italiana (under contract ASI I/088/06/0) and by the Ministero dell’Istruzione, dell’Università e della Ricerca. It is also part of the *Progetti Strategici di Ateneo 2006* granted by the University of Bologna. ED is supported by ASI; he acknowledges the *Marco Polo* programme of the Bologna University for a grant support, and the Department of Astronomy of the University of Virginia for the hospitality during his stay when part of this work was done. RTR is partially supported by STScI grant GO-10524. This research has made use of the ESO/ST-ECF Science Archive facility which is a joint collaboration of the European Southern Observatory and the Space Telescope - European Coordinating Facility.

REFERENCES

- Beccari et al. 2008, in press in the ApJ, (arXiv:0802.2613)
- Bedin, L. R., Piotto, G., Anderson, J., Cassisi, S., King, I. R., Momany, Y., & Carraro, G. 2004, ApJ, 605, L125
- Bekki, K., & Freeman, K. C. 2003, MNRAS, 346, L11
- Bellazzini, M. 2007, A&A, 473, 171
- Buonanno, R., Buscema, G., Corsi, C. E., Ferraro, I., & Iannicola, G. 1983, A&A, 126, 278
- Buonanno, R., & Iannicola, G. 1989, PASP, 101, 294
- Busso, G., et al. 2007, A&A, 474, 105
- Caloi, V., & D’Antona, F. 2007, A&A, 463, 949
- Catelan, M. 2007, ArXiv e-prints, 708, arXiv:0708.2445

- D'Antona, F., Bellazzini, M., Caloi, V., Pecci, F. F., Galleti, S., & Rood, R. T. 2005, *ApJ*, 631, 868
- Davies, M. B., Piotto, G., & de Angeli, F. 2004, *MNRAS*, 349, 129
- Djorgovski, S. 1993, in *ASPC Conf. Ser. 50, Structure and Dynamics of Globular Clusters*, ed. S. G. Djorgovski & G. Meylan (San Francisco: ASP), 373D
- Dalessandro, E., Lanzoni, B., Ferraro, F. R., Rood, R. T., Milone, A., Piotto, G., & Valenti, E. 2007, *ArXiv e-prints*, 712, arXiv:0712.4272
- Federici, L., Bellazzini, M., Galleti, S., Fusi Pecci, F., Buzzoni, A., & Parmegiani, G. 2007, *A&A*, 473, 429
- Ferraro, F. R., Fusi Pecci, F., Cacciari, C., Corsi, C., Buonanno, R., Fahlman, G. G., & Richer, H. B. 1993, *AJ*, 106, 2324
- Ferraro, F. R., Fusi Pecci, F., & Bellazzini, M. 1995, *A&A*, 294, 80
- Ferraro, F. R., Paltrinieri, B., Rood, R. T., & Dorman, B. 1999a, *ApJ* 522, 983
- Ferraro F. R., Messineo M., Fusi Pecci F., De Palo M. A., Straniero O., Chieffi A., & Limongi M. 1999b, *AJ*, 118, 1738
- Ferraro, F. R., Sills, A., Rood, R. T., Paltrinieri, B., & Buonanno, R. 2003, *ApJ*, 588, 464
- Ferraro, F. R., Sollima, A., Pancino, E., Bellazzini, M., Straniero, O., Origlia, L., & Cool, A. M. 2004, *ApJ*, 603, L81
- Ferraro, F. R., Sollima, A., Rood, R. T., Origlia, L., Pancino, E., & Bellazzini, M. 2006, *ApJ*, 638, 433 (F06)
- Harris, W.E. 1996, *AJ*, 112, 1487
- Harris, W. E., et al. 1997, *AJ*, 114, 1030
- Heber, U., Moehler, S., Napiwotzki, R., Thejll, P., & Green, E. M. 2002, *A&A*, 383, 938
- Hills, J. G., & Day, C. A. 1976, *Astrophys. Lett.*, 17, 87
- Lanzoni, B., Dalessandro, E., Ferraro, F. R., Mancini, C., Beccari, G., Rood, R. T., Mapelli, M., & Sigurdsson, S. 2007a, *ApJ*, 663, 267
- Lanzoni, B., et al. 2007b, *ApJ*, 663, 1040

- Lanzoni, B., Dalessandro, E., Perina, S., Ferraro, F. R., Rood, R. T., & Sollima, A. 2007c, *ApJ*, 670, 1065
- Layden, A. C., & Sarajedini, A. 2000, *AJ*, 119, 1760
- Lee, Y.-W., Joo, J.-M., Sohn, Y.-J., Rey, S.-C., Lee, H.-C., & Walker, A. R. 1999, *Nature*, 402, 55
- Mackey, A. D., & van den Bergh, S. 2005, *MNRAS*, 360, 631
- Mapelli, M., Sigurdsson, S., Colpi, M., Ferraro, F. R., Possenti, A., Rood, R. T., Sills, A., & Beccari, G. 2004, *ApJ*, 605, L29
- Mapelli, M., Sigurdsson, S., Ferraro, F. R., Colpi, M., Possenti, A., & Lanzoni, B. 2006, *MNRAS*, 373, 361
- McCrea, W. H. 1964, *MNRAS*, 128, 147
- Meylan, G., & Heggie, D. C. 1997, *A&A Rev.*, 8, 1
- Moehler, S., Sweigart, A. V., Landsman, W. B., Hammer, N. J., & Dreizler, S. 2004, *A&A*, 415, 313
- Monaco, L., Bellazzini, M., Ferraro, F. R., & Pancino, E. 2005, *MNRAS*, 356, 1396
- Montegriffo, P., Ferraro, F. R., Fusi Pecci, F., & Origlia, L. 1995, *MNRAS*, 276, 739
- Newberg, H. J., et al. 2003, *ApJ*, 596, L191
- Pancino, E., Ferraro, F. R., Bellazzini, M., Piotto, G., & Zoccali, M. 2000, *ApJ*, 534, L83
- Pryor C., & Meylan G., 1993, *Structure and Dynamics of Globular Clusters*. Proceedings of a Workshop held in Berkeley, California, July 15-17, 1992, to Honor the 65th Birthday of Ivan King. Editors, S.G. Djorgovski and G. Meylan; Publisher, Astronomical Society of the Pacific, Vol. 50, 357
- Renzini, A., & Fusi Pecci, F. 1988, *ARA&A*, 26, 199
- Rey, S.-C., Lee, Y.-W., Ree, C. H., Joo, J.-M., Sohn, Y.-J., & Walker, A. R. 2004, *AJ*, 127, 958
- Rich, R. M., et al. 1997, *ApJ*, 484, L25
- Ripepi, V., et al. 2007, *ApJ*, 667, L61

Schechter, P. L., Mateo, M., & Saha, A. 1993, *PASP*, 105, 1342

Shara, M. M., Saffer, R. A., & Livio, M. 1997, *ApJ*, 489, L59

Sirianni, M., et al. 2005, *PASP*, 117, 1049

Sollima, A., Pancino, E., Ferraro, F. R., Bellazzini, M., Straniero, O., & Pasquini, L. 2005, *ApJ*, 634, 332

Sollima, A., Lanzoni, B., Beccari, G., Ferraro, F. R., & Fusi Pecci, F. 2008, (arXiv:0801.4511)

van den Bergh, S., & Mackey, A. D. 2004, *MNRAS*, 354, 713

Zinn, R., & Searle, L. 1976, *ApJ*, 209, 734

Table 1. The BSS population of NGC 2419

Name	RA [degree]	DEC [degree]	B	V	I
BSS 1	114.5346238	38.8659223	21.67	21.48	21.19
BSS 2	114.5317934	38.8778178	21.97	21.84	21.60
BSS 3	114.5545324	38.8522824	22.01	21.86	21.55
BSS 4	114.5290061	38.8781085	21.96	21.87	21.78
BSS 5	114.5563785	38.8777071	22.03	21.88	21.67
BSS 6	114.5375980	38.8849180	21.99	21.88	21.70
BSS 7	114.5426076	38.8723283	22.20	21.98	21.72
BSS 8	114.5322465	38.8824554	22.08	21.98	21.86
BSS 9	114.5321660	38.8802393	22.10	21.99	21.81
BSS 10	114.5314467	38.8844550	22.11	21.99	21.72
BSS 11	114.5389799	38.8741541	22.20	22.04	21.83
BSS 12	114.5180869	38.8707066	22.20	22.04	21.88
BSS 13	114.5333262	38.8735631	22.24	22.09	21.62
BSS 14	114.5186506	38.8555156	22.15	22.09	22.05
BSS 15	114.5631273	38.8567423	22.34	22.10	21.72
BSS 16	114.5350018	38.8575038	22.36	22.14	21.79
BSS 17	114.5220854	38.8869184	22.32	22.14	21.83
BSS 18	114.5559528	38.8756214	22.36	22.14	21.82
BSS 19	114.5308496	38.8836661	22.36	22.15	21.86
BSS 20	114.5052076	38.8695694	22.27	22.18	22.06
BSS 21	114.5479750	38.8829417	22.39	22.23	21.98
BSS 22	114.5542824	38.8787225	22.35	22.23	22.04
BSS 23	114.5279917	38.8771869	22.33	22.23	22.05
BSS 24	114.5289397	38.8789566	22.35	22.25	22.22
BSS 25	114.5402618	38.8322954	22.45	22.30	21.80
BSS 26	114.5544769	38.8807888	22.51	22.30	21.96
BSS 27	114.5179647	38.8667478	22.53	22.35	22.06
BSS 28	114.5208423	38.8864626	22.44	22.37	22.17
BSS 29	114.5099740	38.8743802	22.49	22.38	22.18
BSS 30	114.5707475	38.8723047	22.56	22.39	22.14
BSS 31	114.5349532	38.8807603	22.62	22.43	22.14
BSS 32	114.5373408	38.8847449	22.68	22.43	22.06
BSS 33	114.5255999	38.8898043	22.69	22.46	22.23
BSS 34	114.5213599	38.8819734	22.63	22.49	22.32
BSS 35	114.5624518	38.8577883	22.68	22.51	22.22
BSS 36	114.5502354	38.8587983	22.65	22.52	22.29

Table 1—Continued

Name	RA [degree]	DEC [degree]	B	V	I
BSS 37	114.5724785	38.8543265	22.70	22.52	22.22
BSS 38	114.5377048	38.8776849	22.74	22.56	22.38
BSS 39	114.5367933	38.8863131	22.75	22.56	22.25
BSS 40	114.5370632	38.8841385	22.65	22.57	22.41
BSS 41	114.5416913	38.8744374	22.80	22.57	22.20
BSS 42	114.5328193	38.8783052	22.61	22.57	22.29
BSS 43	114.5410755	38.8636039	22.70	22.58	22.35
BSS 44	114.5443444	38.8841840	22.78	22.58	22.18
BSS 45	114.5355871	38.8586443	22.72	22.59	22.29
BSS 46	114.5330413	38.8827233	22.75	22.59	22.34
BSS 47	114.5100504	38.8739744	22.78	22.59	22.38
BSS 48	114.5394051	38.8758936	22.74	22.60	22.44
BSS 49	114.5271347	38.8795152	22.76	22.61	22.42
BSS 50	114.5277051	38.8748074	22.77	22.64	22.42
BSS 51	114.5364186	38.8728954	22.88	22.65	22.22
BSS 52	114.5358544	38.8787353	22.86	22.66	22.44
BSS 53	114.4982285	38.8531324	22.78	22.67	22.14
BSS 54	114.5145126	38.8789390	22.88	22.69	22.41
BSS 55	114.5136075	38.8758341	22.84	22.70	22.50
BSS 56	114.5436548	38.8769220	22.94	22.70	22.35
BSS 57	114.5435517	38.8814084	22.92	22.70	22.40
BSS 58	114.5381816	38.8832314	22.99	22.71	22.25
BSS 59	114.5366860	38.8800032	22.88	22.72	22.39
BSS 60	114.5285765	38.8761503	22.82	22.72	22.40
BSS 61	114.5653514	38.8672278	22.90	22.74	22.41
BSS 62	114.5319576	38.8456597	22.89	22.74	22.52
BSS 63	114.5332823	38.8808548	22.90	22.75	22.50
BSS 64	114.5201658	38.8716290	23.05	22.75	22.49
BSS 65	114.5182917	38.8645682	22.93	22.76	22.43
BSS 66	114.5422667	38.8810701	23.00	22.77	22.48
BSS 67	114.5383605	38.8855947	23.02	22.77	22.42
BSS 68	114.5228769	38.8715036	22.95	22.78	22.58
BSS 69	114.5655782	38.8738971	22.95	22.79	22.54
BSS 70	114.5508635	38.8556174	22.91	22.80	22.44
BSS 71	114.5248251	38.8798819	23.03	22.80	22.50
BSS 72	114.5330946	38.8782802	22.94	22.81	22.42

Table 1—Continued

Name	RA [degree]	DEC [degree]	B	V	I
BSS 73	114.5300473	38.8726778	22.99	22.82	22.42
BSS 74	114.5258531	38.8844487	22.98	22.82	22.57
BSS 75	114.5348296	38.8738382	23.04	22.84	22.40
BSS 76	114.5148586	38.8769283	23.00	22.85	22.74
BSS 77	114.5516168	38.8734430	23.02	22.85	22.62
BSS 78	114.5466460	38.8781617	23.02	22.86	22.60
BSS 79	114.5394030	38.8844577	23.08	22.86	22.43
BSS 80	114.5282537	38.8767212	23.03	22.88	22.50
BSS 81	114.5306900	38.8770293	23.08	22.89	22.55
BSS 82	114.5385251	38.8771382	23.00	22.90	22.66
BSS 83	114.5235814	38.8729527	23.16	22.92	22.48
BSS 84	114.5355456	38.8739955	23.18	22.92	22.46
BSS 85	114.5333547	38.8705373	23.05	22.93	22.76
BSS 86	114.5268290	38.8888513	23.08	22.93	22.65
BSS 87	114.5286345	38.8824567	23.17	22.95	22.57
BSS 88	114.5272080	38.8829733	23.15	22.97	22.68
BSS 89	114.5297549	38.8842508	23.17	22.97	22.74
BSS 90	114.5374061	38.8851489	23.23	22.98	22.72
BSS 91	114.5305231	38.8777378	23.19	22.99	22.63
BSS 92	114.5306248	38.8655249	23.12	23.00	22.44
BSS 93	114.5298495	38.8808827	23.18	23.00	22.55
BSS 94	114.5250029	38.8861768	23.26	23.00	22.62
BSS 95	114.5319072	38.8857620	23.20	23.01	22.75
BSS 96	114.5766634	38.8573333	23.27	23.02	22.64
BSS 97	114.5540530	38.8462298	23.17	23.03	22.62
BSS 98	114.5446661	38.8786382	23.24	23.04	22.85
BSS 99	114.5416242	38.8825834	23.19	23.04	22.57
BSS 100	114.5559916	38.8782646	23.32	23.06	22.67
BSS 101	114.5467694	38.8799242	23.34	23.07	22.71
BSS 102	114.5245139	38.8773725	23.24	23.07	22.71
BSS 103	114.5335661	38.8876156	23.24	23.07	22.85
BSS 104	114.5338201	38.8808881	23.32	23.07	22.79
BSS 105	114.5251903	38.8708786	23.30	23.07	22.63
BSS 106	114.5155847	38.8515763	23.25	23.08	22.62
BSS 107	114.5482144	38.8762432	23.24	23.09	22.69
BSS 108	114.5283801	38.8804424	23.32	23.09	22.73

Table 1—Continued

Name	RA [degree]	DEC [degree]	B	V	I
BSS 109	114.5272202	38.8806563	23.33	23.09	22.75
BSS 110	114.5329037	38.8787814	23.21	23.10	22.82
BSS 111	114.5648250	38.8809186	23.39	23.10	22.67
BSS 112	114.5655476	38.8353859	23.08	23.11	22.62
BSS 113	114.5340609	38.8672425	23.38	23.11	22.72
BSS 114	114.5241875	38.8826388	23.39	23.11	22.76
BSS 115	114.5440484	38.8728605	23.33	23.12	22.70
BSS 116	114.5318474	38.8804939	23.31	23.12	22.82
BSS 117	114.4975565	38.8498301	23.36	23.14	22.69
BSS 118	114.5308869	38.8858920	23.31	23.14	22.65
BSS 119	114.5319236	38.8814812	23.39	23.14	22.77
BSS 120	114.5365736	38.8749561	23.34	23.14	22.74
BSS 121	114.5548031	38.8770840	23.36	23.15	22.84
BSS 122	114.5698279	38.8632929	23.43	23.15	22.88
BSS 123	114.5429103	38.8833364	23.26	23.15	22.81
BSS 124	114.5180654	38.8526066	23.35	23.15	22.81
BSS 125	114.5713938	38.8644595	23.41	23.15	22.81
BSS 126	114.5151887	38.8881692	23.29	23.16	22.85
BSS 127	114.4971710	38.8503894	23.39	23.18	22.80
BSS 128	114.5389324	38.8662627	23.35	23.18	22.72
BSS 129	114.5653667	38.8735289	23.35	23.19	22.80
BSS 130	114.5290415	38.8850904	23.46	23.19	22.82
BSS 131	114.5263335	38.8860022	23.29	23.20	22.80
BSS 132	114.5704264	38.8781784	23.35	23.20	22.91
BSS 133	114.5450942	38.8616024	23.42	23.21	22.90
BSS 134	114.5261968	38.8738325	23.43	23.21	22.75
BSS 135	114.5411974	38.8462718	23.46	23.21	22.85
BSS 136	114.5459761	38.8828031	23.37	23.21	22.86
BSS 137	114.5219796	38.8885754	23.44	23.25	22.97
BSS 138	114.5550069	38.8277938	23.47	23.26	22.97
BSS 139	114.5343111	38.8853578	23.49	23.27	22.86
BSS 140	114.5707653	38.8713824	23.52	23.27	22.85
BSS 141	114.5633208	38.8755186	23.52	23.28	22.91
BSS 142	114.5372475	38.8697969	23.58	23.29	22.83
BSS 143	114.5128112	38.8761214	23.54	23.30	22.95
BSS 144	114.5303288	38.8832148	23.55	23.31	22.99

Table 1—Continued

Name	RA [degree]	DEC [degree]	B	V	I
BSS 145	114.5293403	38.8792390	23.56	23.31	22.81
BSS 146	114.5403815	38.8621857	23.46	23.32	22.93
BSS 147	114.5328409	38.8759082	23.58	23.34	23.02
BSS 148	114.5058275	38.8390039	23.55	23.35	22.96
BSS 149	114.5354601	38.8773111	23.55	23.38	22.94
BSS 150	114.5289120	38.8672031	23.58	23.38	22.88
BSS 151	114.5165945	38.8734688	23.51	23.39	23.01
BSS 152	114.5364602	38.8814663	22.50	22.51	22.27
BSS 153	114.5340522	38.8779415	22.62	22.62	22.42
BSS 154	114.5347666	38.8829015	22.75	22.79	22.62
BSS 155	114.5593850	38.8513222	22.80	22.76	22.40
BSS 156	114.5358572	38.8710266	22.88	22.91	22.47
BSS 157	114.5439332	38.8315146	22.97	22.98	22.51
BSS 158	114.5550096	38.8666358	22.95	22.60	22.59
BSS 159	114.5358955	38.8824612	23.24	22.88	22.63
BSS 160	114.5736822	38.8698082	23.27	22.95	22.64
BSS 161	114.5383375	38.8831536	23.28	22.89	22.53
BSS 162	114.5363135	38.8768683	23.34	22.97	22.70
BSS 163	114.5411630	38.8818491	23.37	22.99	22.73
BSS 164	114.5385990	38.8814390	23.46	23.16	22.74
BSS 165	114.5303744	38.8839579	23.53	23.22	22.90
BSS 166	114.5342489	38.8869653	23.55	23.52	23.12
BSS 167	114.5326253	38.8762184	23.56	23.18	22.82
BSS 168	114.5274273	38.8465093	22.44	22.52	22.09
BSS 169	114.5294680	38.8762898	21.67	-	21.58
BSS 170	114.5590138	38.8529876	22.61	-	22.13
BSS 171	114.5352678	38.8831155	23.27	-	22.54
BSS 172	114.5293589	38.8824958	23.28	-	22.54
BSS 173	114.5331303	38.8781672	22.37	-	21.82
BSS 174	114.5372462	38.8804816	22.38	-	21.92
BSS 175	114.5371350	38.8825563	23.11	-	22.68
BSS 176	114.5299404	38.8833588	23.03	-	22.66
BSS 177	114.5377141	38.8839299	22.28	-	21.96
BSS 178	114.5318896	38.8816916	23.40	-	22.72
BSS 179	114.5338975	38.8878113	22.30	-	21.76
BSS 180	114.5354840	38.8848507	21.99	-	21.99

Table 1—Continued

Name	RA [degree]	DEC [degree]	B	V	I
BSS 181	114.5416767	38.8787643	22.16	-	21.86
BSS 182	114.5274273	38.8465093	22.44	-	22.09
BSS 183	114.5430587	38.8788861	22.52	-	22.27
BSS 184	114.6046393	38.8739340	-	21.61	21.50
BSS 185	114.4732159	38.8794161	-	22.22	22.11
BSS 186	114.5948464	38.8317186	-	22.29	22.18
BSS 187	114.4921101	38.8826003	-	22.36	22.13
BSS 188	114.4795474	38.8950070	-	22.42	22.00
BSS 189	114.5742838	38.8787606	-	22.51	22.11
BSS 190	114.5769900	38.8517555	-	22.53	22.25
BSS 191	114.5235357	38.9041986	-	22.57	22.32
BSS 192	114.6028209	38.8986391	-	22.59	22.26
BSS 193	114.5780235	38.8817962	-	22.63	22.39
BSS 194	114.5205417	38.9003089	-	22.65	22.44
BSS 195	114.5574956	38.8950661	-	22.68	22.37
BSS 196	114.6020290	38.8716163	-	22.69	22.43
BSS 197	114.4870399	38.8486762	-	22.73	22.39
BSS 198	114.5278361	38.9056871	-	22.74	22.37
BSS 199	114.4868008	38.8777003	-	22.75	22.48
BSS 200	114.5698058	38.8856298	-	22.80	22.43
BSS 201	114.5631611	38.9001108	-	22.80	22.45
BSS 202	114.5728569	38.9152703	-	22.80	22.53
BSS 203	114.5344124	38.9094217	-	22.82	22.45
BSS 204	114.4987279	38.9233287	-	22.84	22.50
BSS 205	114.4950878	38.9045856	-	22.90	22.61
BSS 206	114.5542729	38.8926652	-	22.93	22.61
BSS 207	114.4846796	38.8934777	-	22.96	22.63
BSS 208	114.4793021	38.8865969	-	22.96	22.81
BSS 209	114.4748604	38.9055783	-	22.98	22.61
BSS 210	114.5080023	38.9026343	-	22.97	22.72
BSS 211	114.5573887	38.8903576	-	22.98	22.63
BSS 212	114.5204611	38.9028901	-	23.08	22.85
BSS 213	114.5705620	38.8861123	-	23.09	22.81
BSS 214	114.5548202	38.9085582	-	23.11	22.72
BSS 215	114.5422886	38.8977372	-	23.12	22.84
BSS 216	114.4864816	38.8823681	-	23.16	22.77

Table 1—Continued

Name	RA [degree]	DEC [degree]	B	V	I
BSS 217	114.5658903	38.8861262	-	23.17	22.84
BSS 218	114.5066897	38.8939685	-	23.20	22.79
BSS 219	114.4888325	38.8881818	-	23.27	22.80
BSS 220	114.5077125	38.9123421	-	23.27	22.81
BSS 221	114.4809893	38.8830761	-	23.27	23.04
BSS 222	114.5560389	38.8862473	-	23.29	23.07
BSS 223	114.4463878	38.8771839	-	22.20	22.10
BSS 224	114.3957223	38.8532619	-	22.65	22.27
BSS 225	114.4183885	38.8968389	-	22.86	22.52
BSS 226	114.4386092	38.8140150	-	22.90	22.59
BSS 227	114.3704635	38.8294846	-	23.09	22.73
BSS 228	114.5111720	38.9412987	-	22.61	22.43
BSS 229	114.5357260	39.0140900	-	22.74	22.47
BSS 230	114.4848049	38.9588305	-	22.99	22.67
BSS 231	114.7046122	38.8578500	-	22.18	21.92
BSS 232	114.6843307	38.9221184	-	23.28	22.83

Table 2. Number Counts of BSS, HB, and RGB Stars, and Fraction of Sampled Luminosity

r_i''	r_e''	N_{BSS}	N_{HB}	N_{RGB}	$L^{\text{samp}}/L_{\text{tot}}^{\text{samp}}$
0	20	56	160	745	0.21
20	60	71	253	1137	0.31
60	100	41	142	592 (1)	0.21
100	180	43 (1)	121 (1)	497 (3)	0.18
180	500	15 (5)	77 (11)	248 (27)	0.09

Note. — The values listed out of the parenthesis correspond to the number of stars assumed to belong to the cluster (and thus used in the analysis), while those in the parenthesis are estimated to be contaminating field stars (see Sect. 4.2).

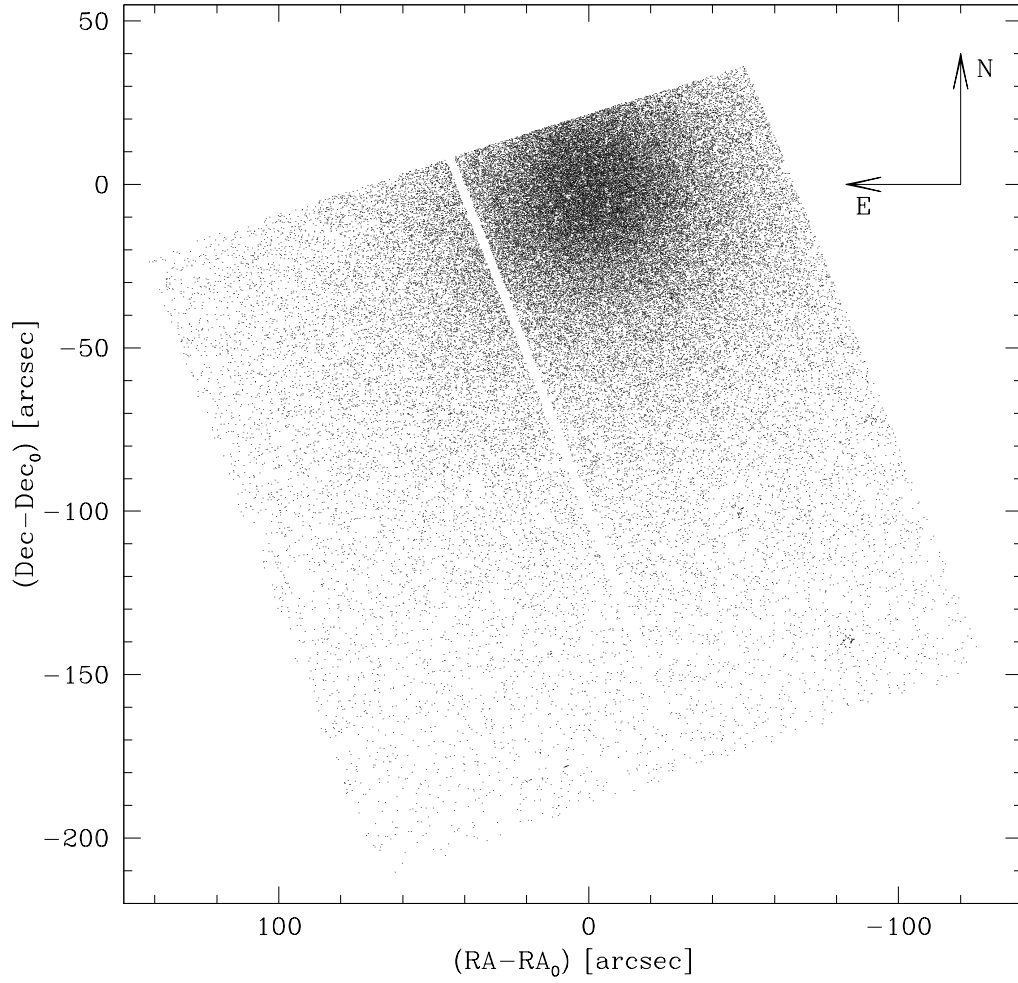


Fig. 1.— Map of the *HST* sample. RA_0 and Dec_0 are the right ascension and the declination of the center of gravity of the cluster.

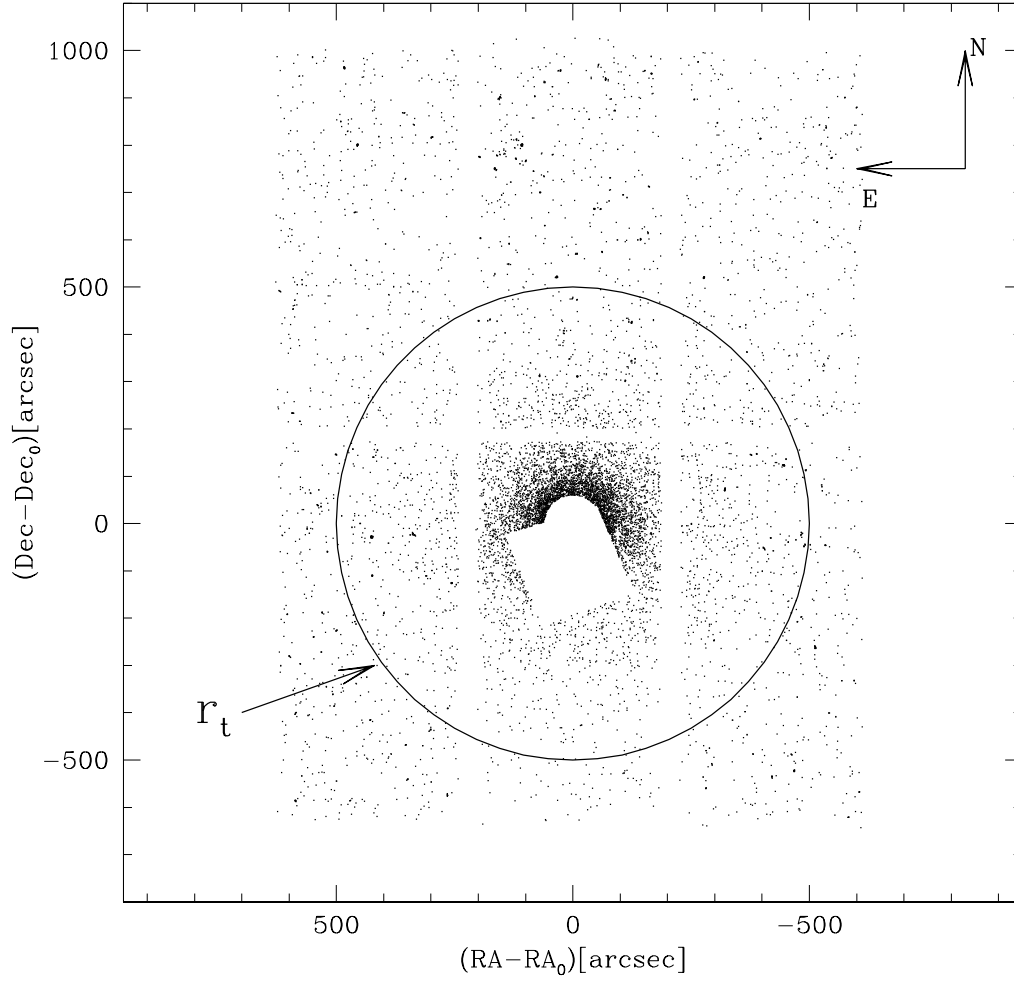


Fig. 2.— Map of the *SUBARU* sample. The circle with radius $r_t = 500''$ (adopted as tidal radius) centered in the cluster center is shown as a solid line.

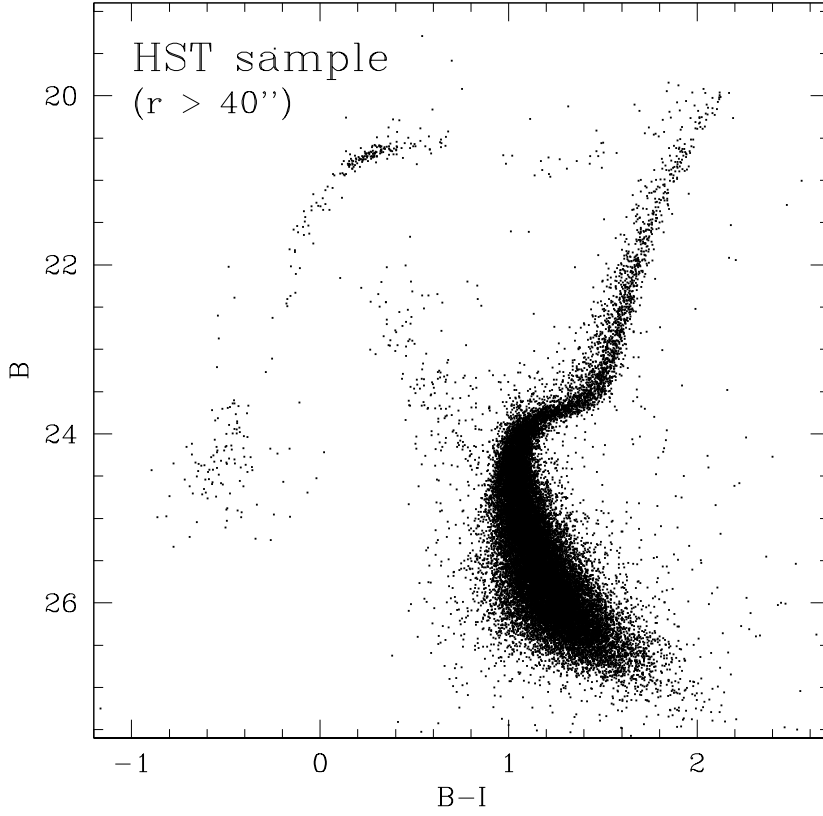


Fig. 3.— $(B, B - I)$ CMD of the *HST* sample for $r > 40''$ from the center, reaching down $B \sim 27$.

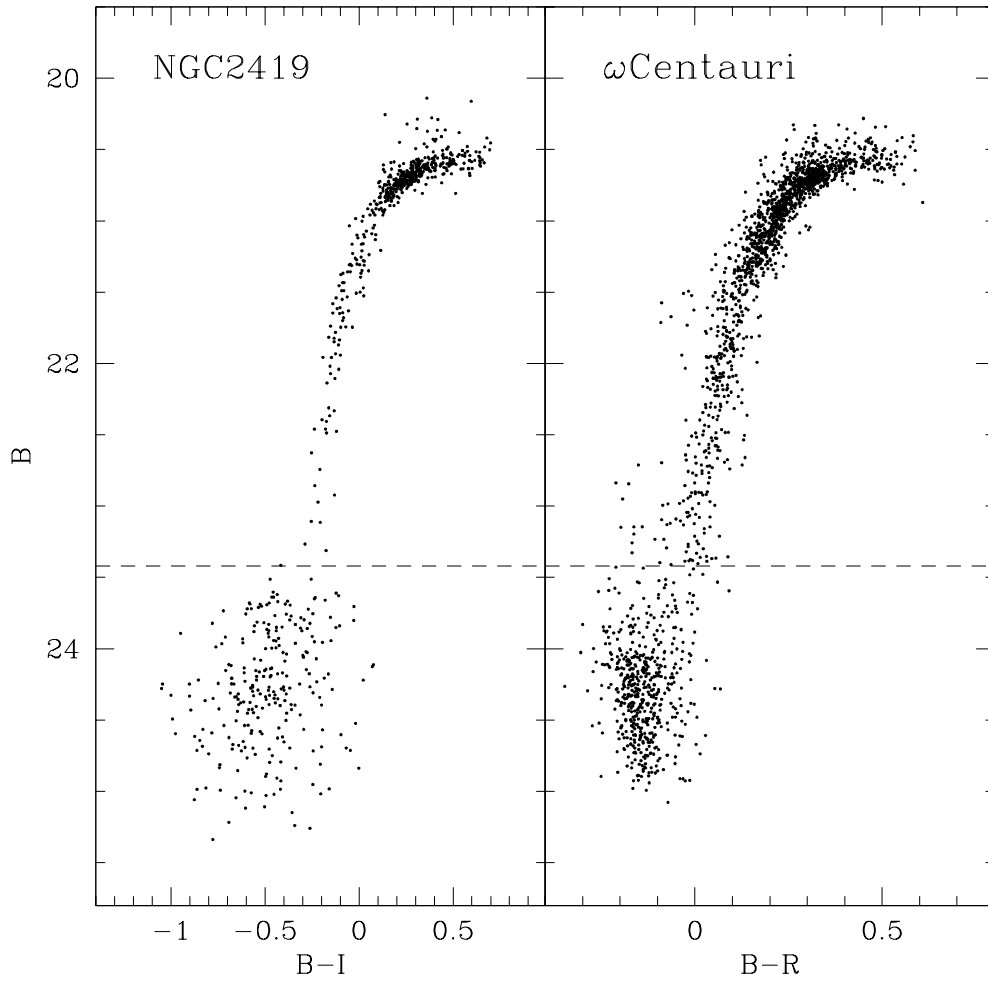


Fig. 4.— Comparison of the HB morphology of NGC 2419 and ω Cen (from F06). Only stars in the ACS FoV are plotted. The HB of ω Cen has been shifted by $\delta B = 5.6$ to match that of NGC 2419. The dashed line marks the brightest boundary of the BHk population.

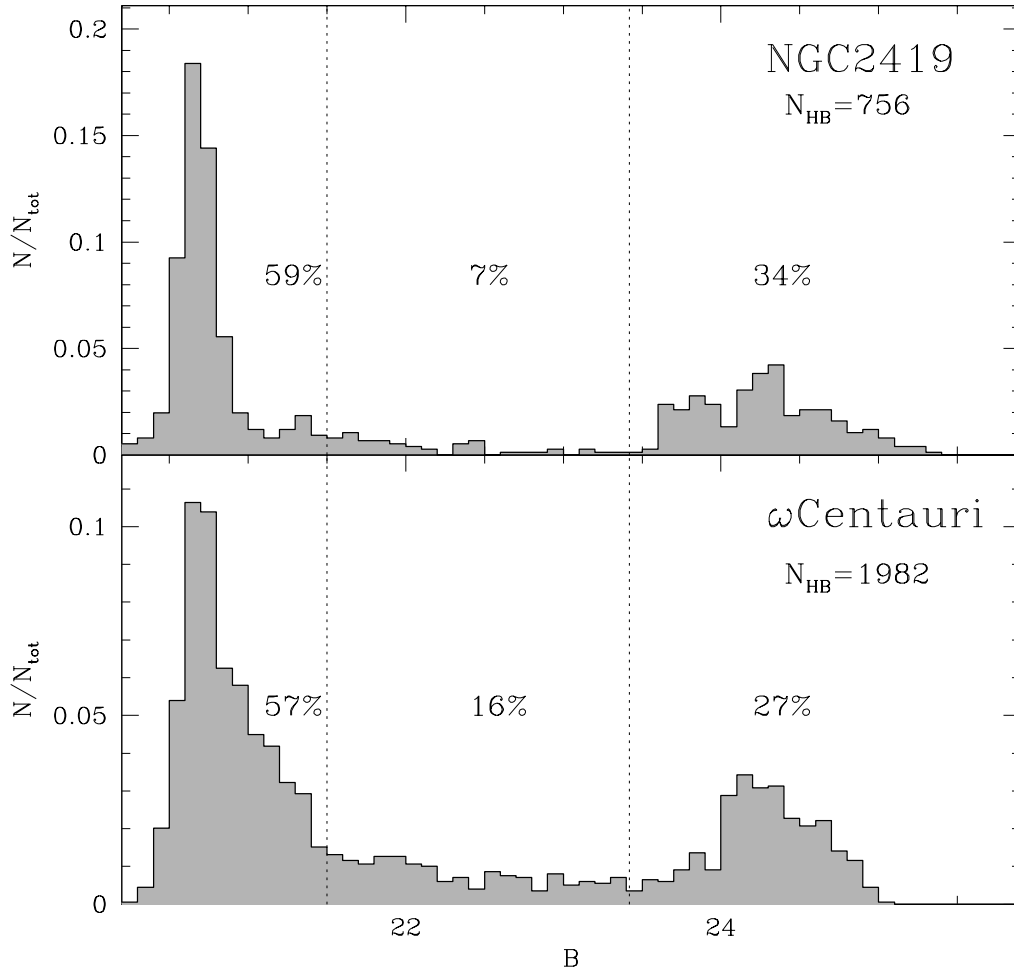


Fig. 5.— Normalized magnitude distributions of the HB stars of NGC 2419 (upper panel) and ω Cen (bottom panel, from F06) plotted in Fig. 4. The vertical dotted lines mark three (arbitrary) portions of the HB separating the bulk of the population, the BT HB and the BHk.

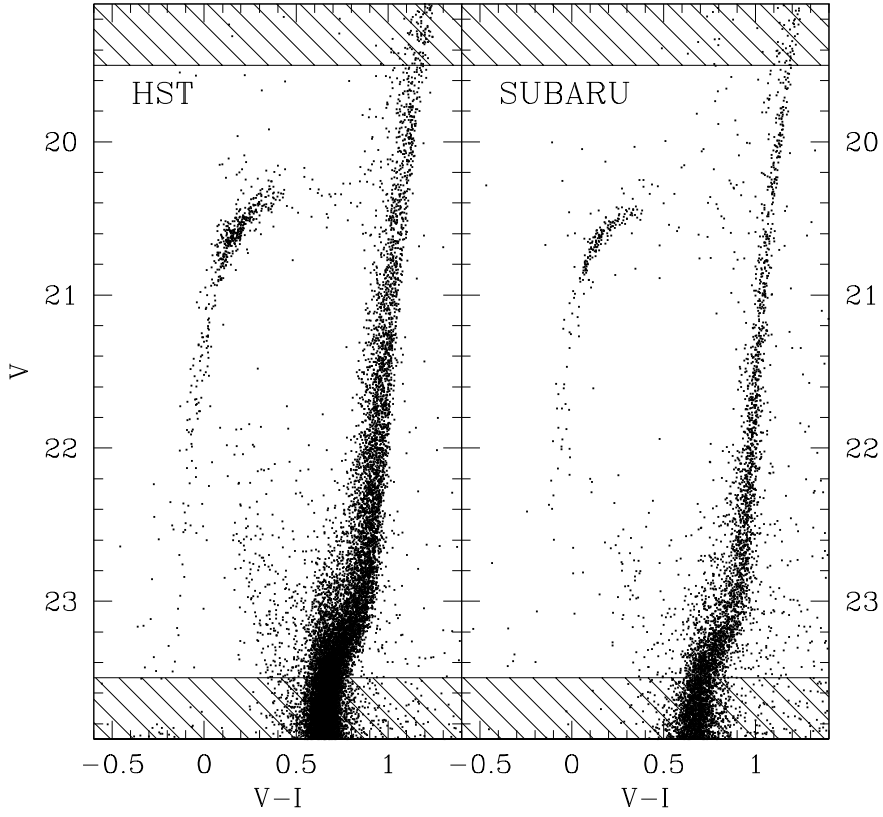


Fig. 6.— CMDs used to derive the surface density profile of NGC 2419. The hatched regions indicate stars that have been excluded because they are saturated in the *HST* sample (those with $V < 19.5$), or in order to avoid incompleteness effects (stars fainter than $V = 23.5$).

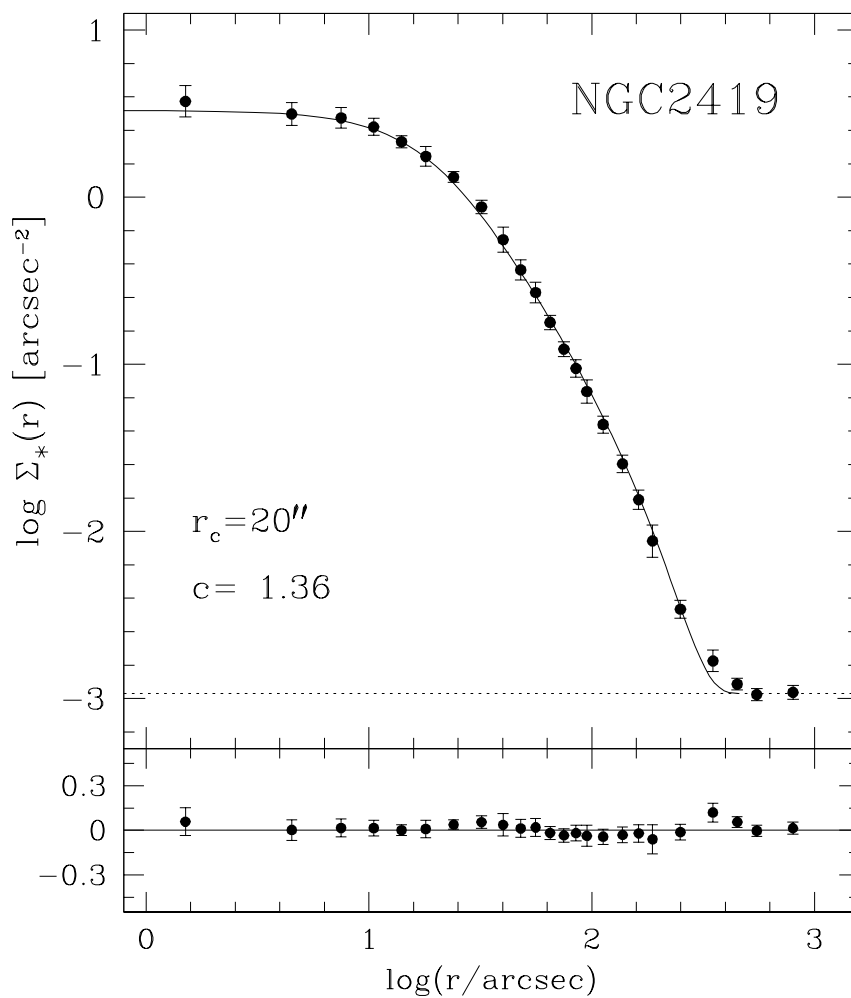


Fig. 7.— Observed surface density profile (*dots and error bars*) and best-fit King model (*solid line*). The radial profile is in units of number of stars per square arcseconds. The *dotted line* indicates the adopted level of the background (corresponding to ~ 4 stars/arcmin²), and the model characteristic parameters (core radius r_c and concentration c) are marked in the figure. The lower panel shows the residuals between the observations and the fitted profile at each radial coordinate.

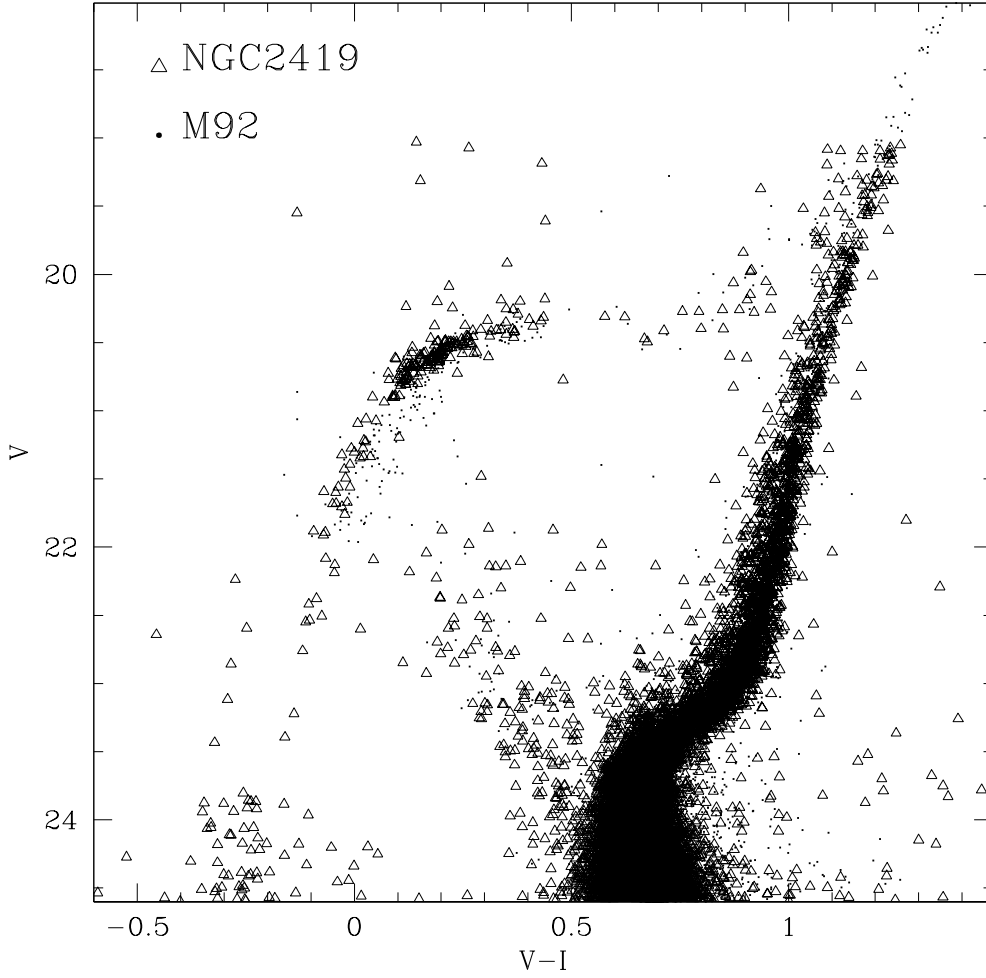


Fig. 8.— $(V, V - I)$ CMD of M92 (*dots*) superimposed onto that of NGC 2419 (*triangles*) after a magnitude shift of $\delta V = 5.25$ and a color shift of $\delta(V - I) = 0.14$.

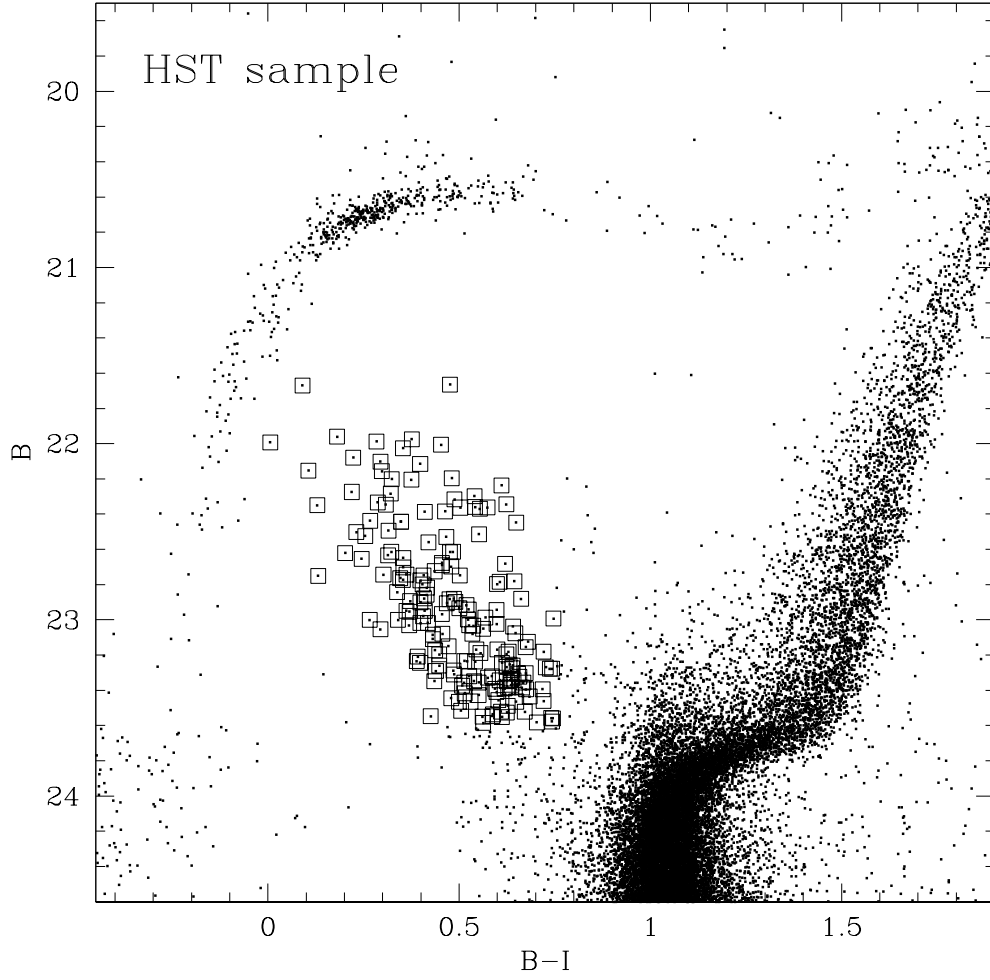


Fig. 9.— BSS population (squares) selected in the $(B, B - I)$ CMD of the *HST* sample.

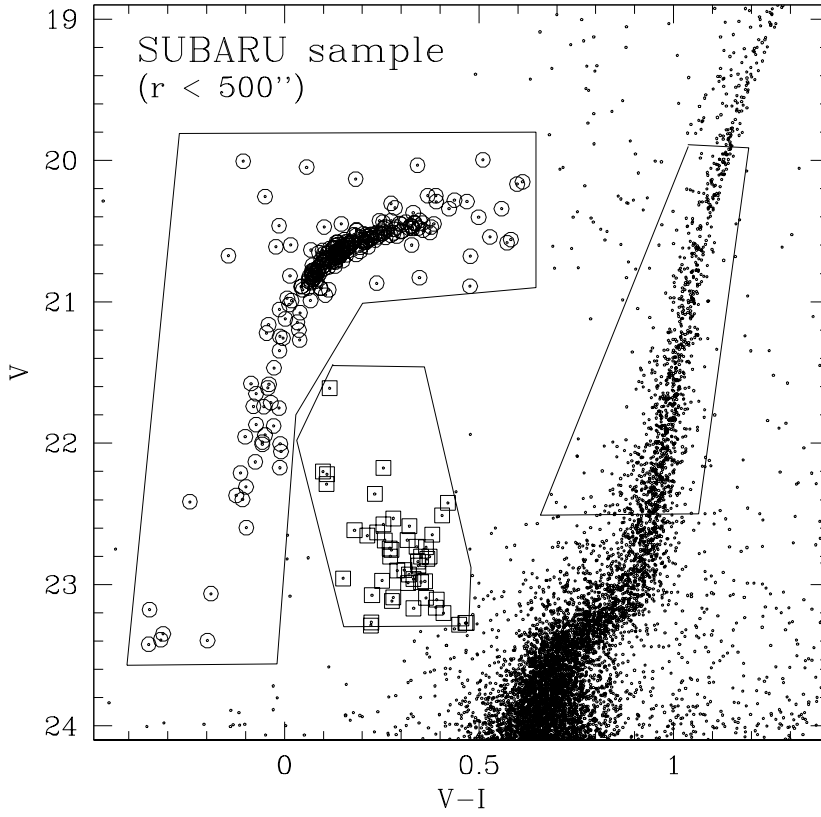


Fig. 10.— $(V, V - I)$ CMD of the SUBARU sample for $r < 500''$ from the center, with the adopted BSS, HB and RGB selection boxes highlighted. The selected BSS and HB populations are also marked with open squares and circles, respectively.

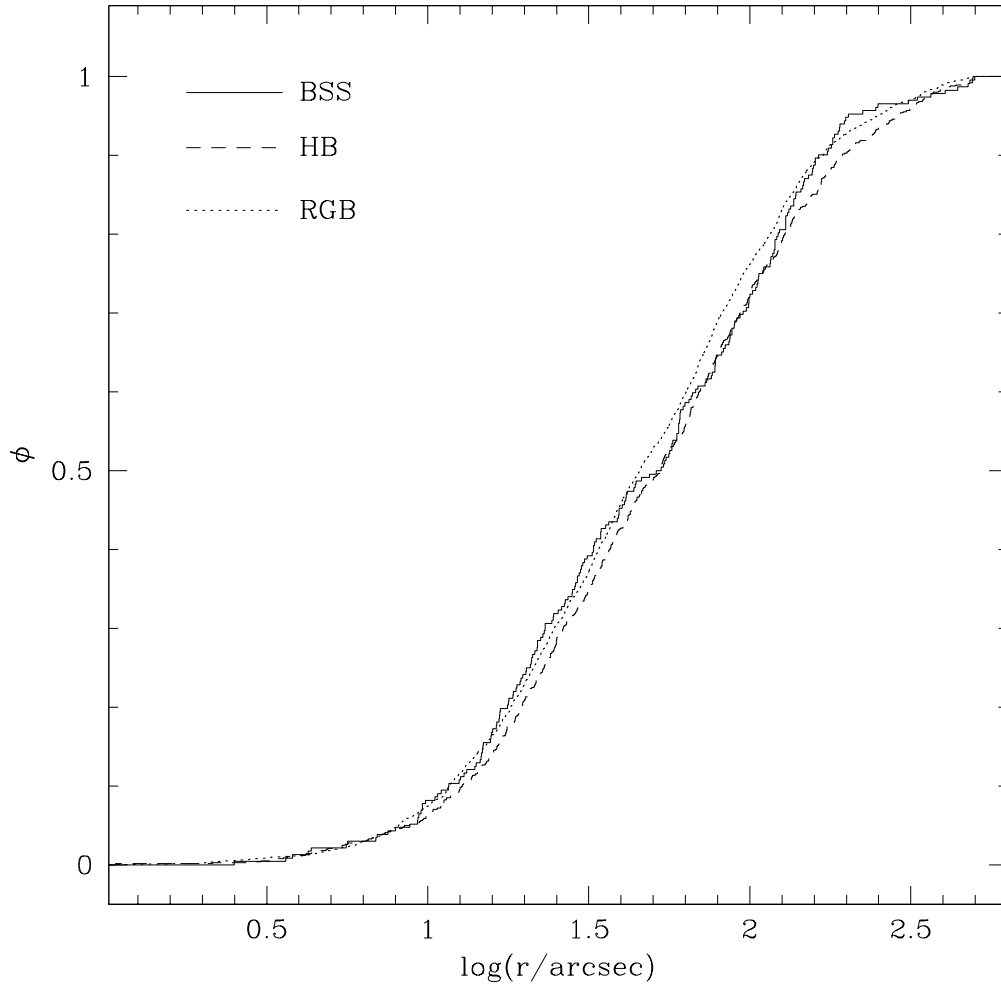


Fig. 11.— Cumulative radial distribution of BSS (solid line), HB (dashed line) and RGB stars (dotted line) as a function of the projected distance from the cluster center, for the combined HST+SUBARU sample at $r < 500''$. The populations show essentially the same radial distribution.

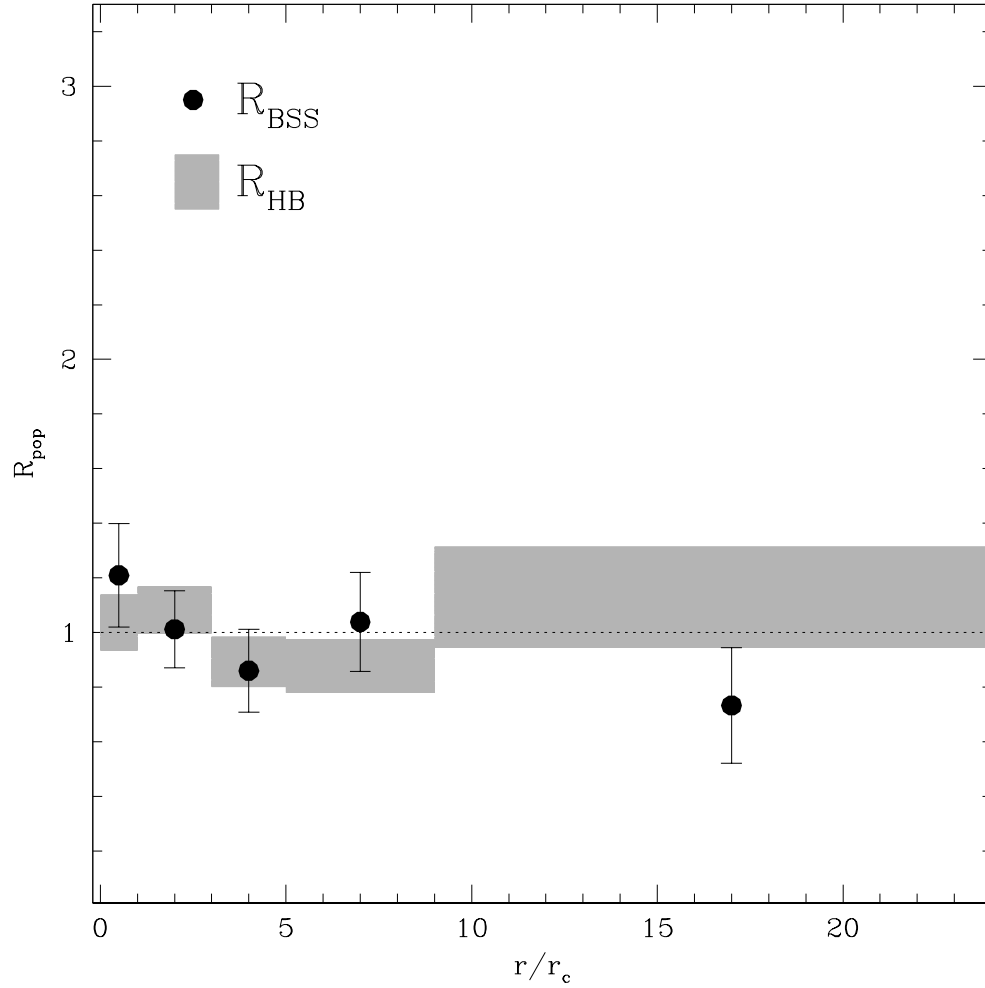


Fig. 12.— Double normalized ratios, as defined in eq. (3), of BSS (dots) and HB stars (grey rectangular regions), plotted as a function of the radial coordinate expressed in units of the core radius. The vertical size of the grey rectangles corresponds to the error bars. The two distributions are almost constant around unity over the entire cluster extension, as expected for any normal, non-segregated cluster population.

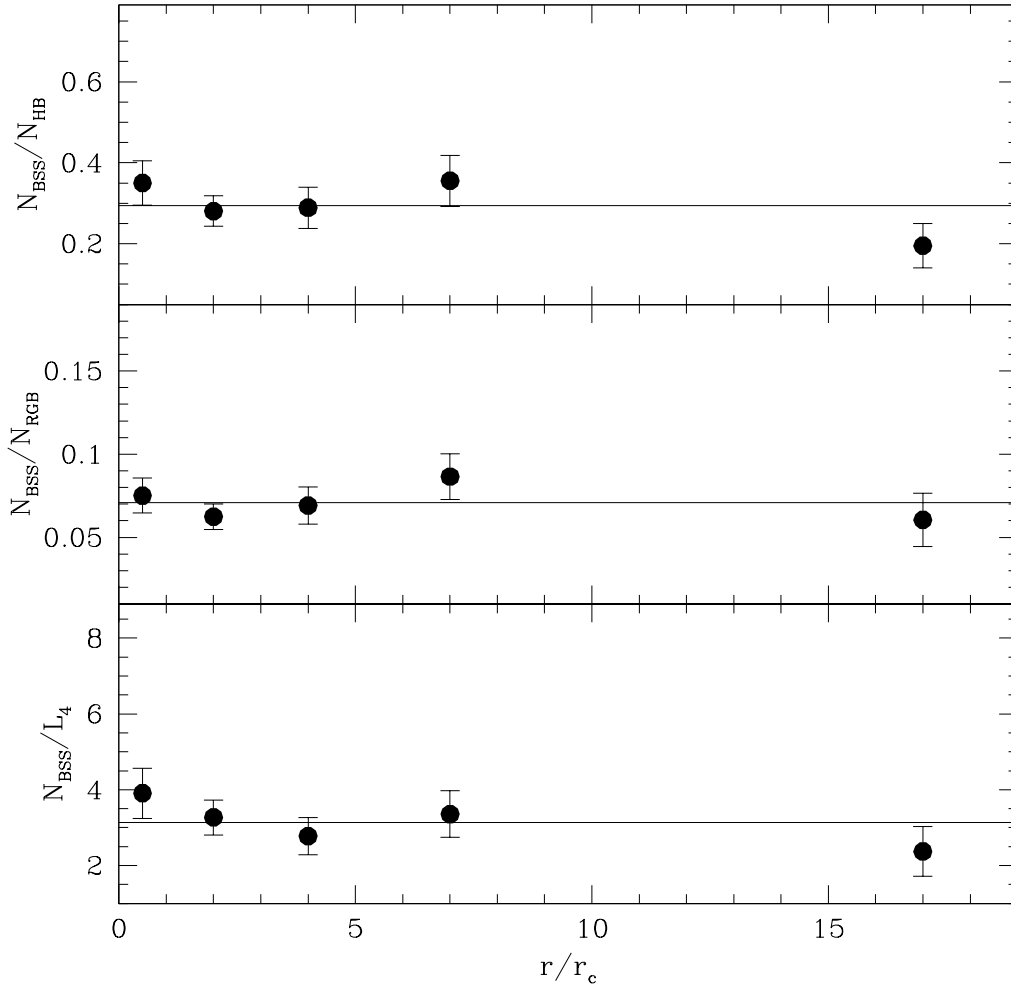


Fig. 13.— Specific frequency of BSS with respect to HB stars (upper panel), RGB stars (middle panel), and the sampled luminosity in units of $10^4 L_\odot$ (bottom panel) as a function of the projected distance from the cluster center in units of r_c .